Role of alkali cations for the excited state dynamics of liquid water near the surface

Franziska Buchner, Hans-Hermann Ritze, Marcus Beutler, Thomas Schultz, Ingolf V. Hertel, and Andrea Lübcke

Citation: The Journal of Chemical Physics **137**, 024503 (2012); doi: 10.1063/1.4732582

View online: http://dx.doi.org/10.1063/1.4732582

View Table of Contents: http://scitation.aip.org/content/aip/journal/jcp/137/2?ver=pdfcov

Published by the AIP Publishing

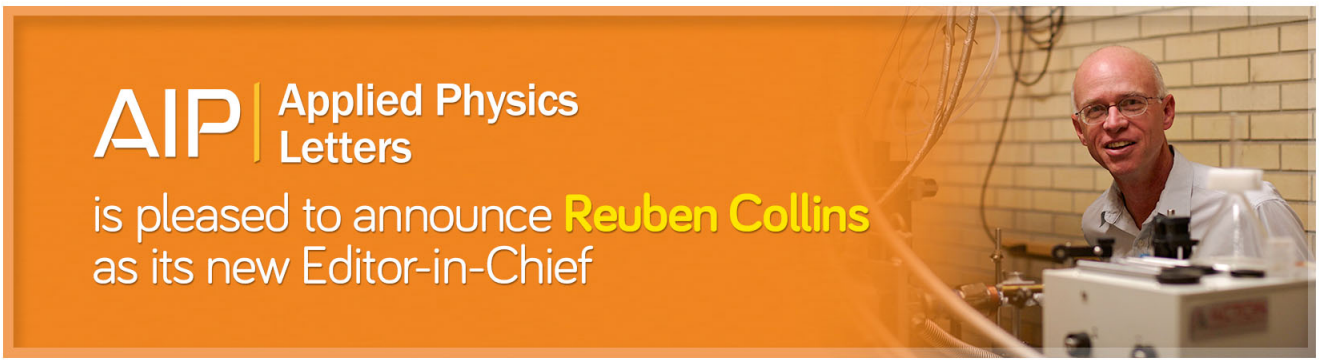

Role of alkali cations for the excited state dynamics of liquid water near the surface

Franziska Buchner, Hans-Hermann Ritze, Marcus Beutler, Thomas Schultz, Ingolf V. Hertel,[a] and Andrea Lübcke[b]
Max-Born-Institut für nichtlineare Optik und Kurzzeitspektroskopie, Max-Born-Strasse 2a, 12489 Berlin, Germany

(Received 25 January 2012; accepted 14 June 2012; published online 11 July 2012)

Time-resolved liquid jet photoelectron spectroscopy was used to explore the excited state dynamics at the liquid water surface in the presence of alkali cations. The data were evaluated with the help of *ab initio* calculations on alkali-water clusters and an extension of these results on the basis of the dielectric continuum model: 160 nm, sub-20 fs vacuum ultraviolet pulses excite water molecules in the solvent shell of Na^+ or K^+ cations and evolve into a transient hydrated complex of alkali-ion and electron. The vertical ionization energy of this transient is about 2.5 eV, significantly smaller than that of the solvated electron. © *2012 American Institute of Physics*. [http://dx.doi.org/10.1063/1.4732582]

I. INTRODUCTION

Despite the fundamental importance of liquid water in all natural sciences, the excited state properties and dynamics of liquid water remain poorly understood. This is mainly due to the fact that the lifetime of the primary excited state is very short—less than 100 fs [1]—and that the transition to the first excited state ($\tilde{X} \rightarrow \tilde{A}$) lies in the vacuum ultraviolet (VUV) region. Whereas, in the gas phase, the corresponding band peaks at 7.45 eV (Ref. 2), and in liquid water, the band maximum is near 8.4 eV (Ref. 3). This blueshift is mainly caused by the large spatial extension of the $4a_1$ Rydberg orbital and the appearance of hydrogen bonds. As pointed out in the literature,[4] the lowest excitation energies in the liquid are associated with broken acceptor hydrogen bonds. Hence, at the surface, a lowering of the absorption edge can be expected. This also implies that the absorption occurs preferentially at the water surface, if the photon energy is below 8 eV. At photon energies $\leq$8.3 eV, the main photoinduced process in pure water is photodissociation. The generation of solvated electrons is only a minor channel, which becomes more important at higher photon energies.[5]

In water, already at photon energies lower than 8 eV, the proximity of cations may enable the direct excitation of a charge transfer state, leading to the formation of transient hydrated cation-electron complexes. In particular, a surface-solvated electron may be temporarily stabilized by subjacent cations.

As has recently been demonstrated in pure water clusters,[6] a high time resolution is desirable to investigate photoinduced processes in water. We have shown that liquid jet photoelectron spectroscopy at low kinetic energies is surface sensitive.[7] Hence, our experiment is well suited to identify surface-specific transient species in photoexcited salt solutions.

In the present work, we report on the investigation of the excited state of liquid water—under the influence of ions—in the vicinity of the liquid to vacuum interface. Our approach uses time-resolved photoelectron spectroscopy[8] with improved time resolution (<20 fs) and 7.75 eV photon energy to characterize electron binding energies and lifetimes of *transient* species in different photoexcited alkali halide solutions. A similar technique has been applied recently to study the solvated electron and charge-transfer-to-solvent (CTTS) dynamics after excitation at lower photon energies.[9–12]

Figure 1 shows the different excited states of all species present in the sample solutions. While the CTTS states of interest in the recent time-resolved photoelectron studies are not accessible by 7.75 eV photons, the higher CTTS states are.

Here, we will show that not only the conventional metastable solvated electron is generated by the excitation of CTTS states, but that the presence of cations also leads to the formation of a transient hydrated electron cation complex $(M^+ \ldots e^-)_{aq}$ at the liquid to vacuum interface. This complex is generated by the excitation of a water molecule in the vicinity of an alkali cation M^+. We will study the temporal evolution of the vertical ionization energy (VIE) of this complex in D_2O and H_2O, the effect of anion and cation variation, as well as the population dynamics. To interpret our experimental results and support our conclusions, we explore the nature of the observed surface-specific transient species by *ab initio* calculations for sodium-water clusters. These *ab initio* results are extrapolated by a dielectric continuum polarization model to describe specific properties at the water surface.

II. EXPERIMENTAL

A commercial Ti:sapphire amplifier system operating at 1 kHz repetition rate (Spitfire Pro) produced 800 nm pulses with a pulse duration of 40 fs and a pulse energy of 3 mJ. VUV pulses with a wavelength of 160 nm were generated in a four-wave mixing process, as described in detail elsewhere.[24,25] To substantially shorten the pulse duration for the pump probe

[a] Also at Institut für Physik, Humboldt-Universität zu Berlin, Newtonstr. 15, D-12489 Berlin-Adlershof, Germany.
[b] Author to whom correspondence should be addressed. Electronic mail: luebcke@mbi-berlin.de.

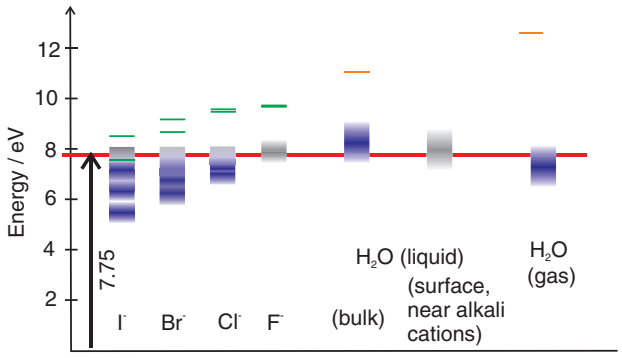

FIG. 1. Excited states in the proximity of the excitation photon energy of 7.75 eV. The energies of the CTTS bands of the halides (blue) are from Refs. 13–16. The band structure (intensities, energy) for large photon energies (≥7.5 eV) is not very well known and thus displayed in grey and only up to ~8 eV. The lowest vertical detachment energies (green) are from Ref. 17, the spin orbit splitting of CTTS bands and vertical photodetachment energies are from Refs. 18–21. For all halides, absorption of 7.75 eV photons is possible. The energy of the water Ã-band (blue) in bulk stems from Ref. 3, and for the gas phase, from Ref. 2. The position of the Ã-band in the vicinity of the surface and an alkali cation is from our own calculations. The vertical ionization energy (orange) of bulk water is from Ref. 22 and for water vapor, from Ref. 23.

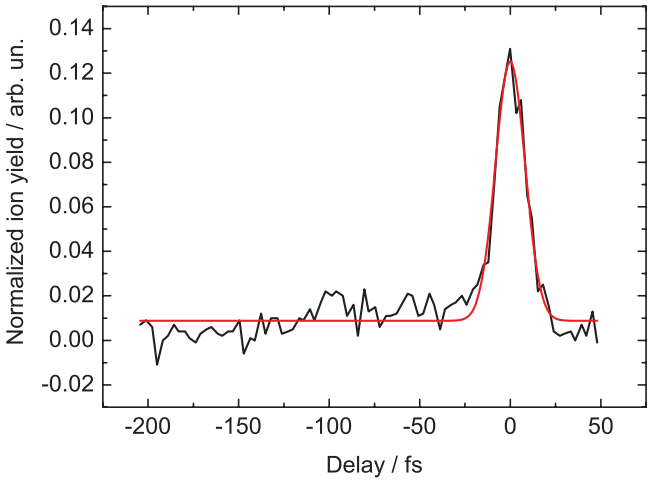

FIG. 2. Cross-correlation trace between the VUV (160 nm) and the fundamental (800 nm) radiation by two-color ionisation of xenon gas. The curve shows the ion yield as a function of delay between both pulses.

experiments, we used the technique of spectral broadening by filamentation in a noble gas-filled cell.[26] By focussing half of the amplifier output into an argon filled gas tube (pressure: 1.1 bars) and 6 bounces of a pair of chirped mirrors, we generated pulses with a spectral bandwidth of about 100 nm, a duration of 13.4 fs, and about 250 μJ of pulse energy. The other half of the amplifier output was sent through nonlinear crystals to generate about 200 μJ of third harmonic (266 nm) with a small bandwidth and a pulse duration of 90 fs. Both pulses were non-collinearly focused into a second argon-filled chamber. With an angle of about 10 mrad between both pulses, we obtained phase matching at about 300 mbar argon pressure and generated up to 400 nJ pulses at 160 nm (Ref. 27).

To evaluate the temporal shape of the VUV pulses, a cross-correlation experiment between the VUV and the fundamental was performed. Two-color ionization of xenon gas in a time-of-flight (TOF) mass spectrometer created a nonlinear signal in a $(1+3)$ process. The ion yield of xenon was measured depending on the temporal delay between the VUV and the fundamental pulse.

As can be seen in Fig. 2, the cross-correlation signal has a Gaussian shape and a width of 19.5 fs (FWHM). A pedestal with a width of about 100 fs and 10% to 20% of the peak power appears prior to time zero. Considering only the main peak, we derive a pulse duration of 18 fs for the VUV pulses using the formula $\tau_{\mathrm{VUV}} = \sqrt{\tau_{\mathrm{xcorr}}^2 - \tau_{\mathrm{Probe}}^2/3}$.

About 70 nJ of the VUV pulses at 160 nm were focused onto a liquid microjet of aqueous alkali halide solution to trigger a photoreaction. At low salt concentration, electrokinetic charging leads to significant potentials shifts and affects measured photoelectron kinetic energies.[8,28] To suppress electrokinetic charging of the liquid jet, the salt concentration was chosen larger than 10 mM. Delayed pulses at 800 nm or 400 nm probed the photoexcited species by photoionization. A detailed description of the time-resolved photoelectron spectrometer can be found in a recent paper.[8] Briefly, a liquid microjet in vacuum, with 10 μm jet diameter, was generated by pushing an aqueous solution through a fused silica nozzle using a high-pressure liquid chromatography (HPLC) pump. The speed of the liquid jet was typically 50 m/s. After several millimeters of laminar flow, the jet broke apart into droplets, but experiments were always performed in the region of laminar flow. The jet passed about 1 mm beneath a 500 μm orifice, which led into the TOF electron spectrometer. The small orifice allowed for efficient differential pumping of the spectrometer. Three liquid nitrogen cold traps in the main chamber froze out the liquid phase and the water vapor. A magnetic bottle ensured the efficient collection of photoelectrons.

III. EXPERIMENTAL RESULTS

A. Short time dynamics in H_2O and D_2O

In Figure 3, we show the time-resolved photoelectron spectra for 30 mM solutions of NaCl in H_2O (left) and D_2O (right). A 400 nm probe pulse was used in the photoionization step. Signals due to one-color, multi-photon ionization were measured separately and subtracted. At negative delays, the photoelectron signal is nonzero due to the pedestal of the VUV pulse (cf. Figure 2). The spectral shape is not well described by a single Gaussian. For this reason, we describe our observation in terms of the average kinetic energy (AKE)

$$\mathrm{AKE} = \frac{\int_0^\infty E_{\mathrm{kin}} I(E_{\mathrm{kin}}) \mathrm{d}E_{\mathrm{kin}}}{\int_0^\infty I(E_{\mathrm{kin}}) \mathrm{d}E_{\mathrm{kin}}}, \quad (1)$$

which does not require any assumption on the spectral shape. We will show below that this band arises from one-photon ionization with the probe pulse.

At the temporal overlap, a photoelectron band appears with AKE = 0.92 eV for the H_2O solution and AKE

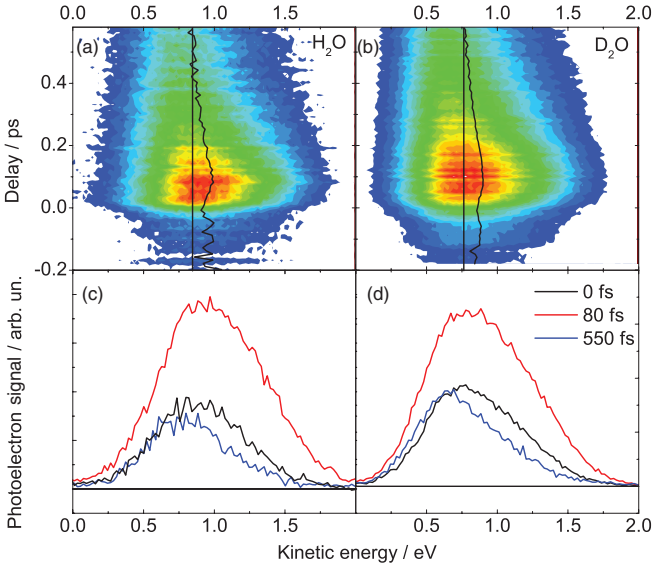

FIG. 3. Time-resolved photoelectron spectra of a 30 mM solution of NaCl in (a) H_2O and in (b) D_2O. The wiggly black curves show the temporal evolution of the average kinetic energy of the photoelectron band. For clarity, a straight line (constant kinetic energy) is also shown. Photoelectron spectra for three selected pump-probe delays are shown for H_2O and D_2O in (c) and (d), respectively. Pump pulse: 160 nm (7.75 eV); probe pulse: 400 nm (3.1 eV).

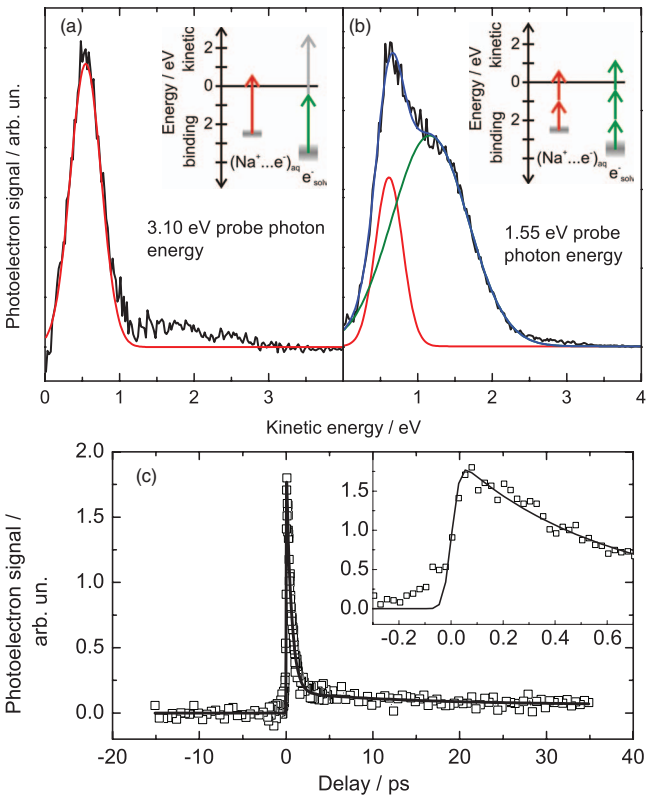

FIG. 5. Time-integrated photoelectron band for an aqueous NaBr solution probed (a) with 400 nm probe pulses and (b) with 800 nm probe pulses. The red and green lines show Gaussian fits to the spectrum. The photoelectron signal was integrated for 5 ps $< \Delta t <$ 30 ps, a temporal region where the photoelectron spectrum remains essentially unchanged. The insets show the energetic situation: The weakly bound species (which we will later assign to the $(M^+ \ldots e^-)_{aq}$ complex) is photoionized by one 3.1 eV photon (a) or two 1.55 eV photons (b). The stronger bound species (we will discuss later that this is probably the conventional solvated electron e^-_{solv}) cannot be photodetached by a single 3.1 eV photon (400 nm); a two-photon process is not observed in this case. With 1.55 eV, a three-photon process occurs. The time-dependent photoelectron signal (integrated over all kinetic energies), probed at 400 nm, is shown in (c).

= 0.86 eV for the D_2O solution. As shown in Figure 4(a), the AKE very quickly shifts toward larger values. For both solutions, the shift is maximal after about 85 fs, when AKE $\sim$ 1.0 eV in H_2O and $\sim$0.9 eV in D_2O. For longer delay times, the AKE shifts toward smaller kinetic energies, i.e., the VIE is increased. The photoelectron signal is present only for very short time delays. In Figure 4(b), we present the energy integrated signal as a function of delay time. This signal can be well fitted by two components: a component with mono-exponential decay and a long-lived component. The limited delay range of these data sets does not allow a reliable fit of the branching ratio between long-lived and short-lived population. Fixing the branching ratio between the short-lived and long-lived population to 97% (as motivated from the results for aqueous NaBr solution discussed later) yields a lifetime of (330 $\pm$ 10) fs for H_2O and (430 $\pm$ 20) fs for D_2O. It is remarkable that the lifetime in D_2O is about 1.3 times longer than in H_2O, thus, we observe a distinct isotope effect of the population dynamics.

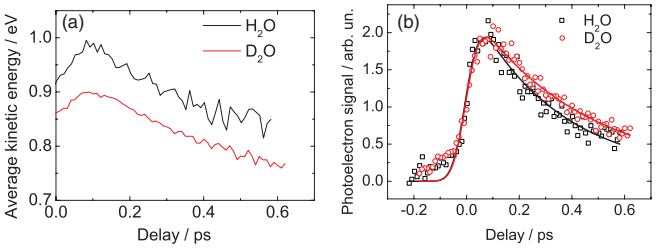

FIG. 4. (a) Temporal evolution of the average kinetic energy and (b) the spectrally integrated photoelectron signal for a 30 mM solution of NaCl in H_2O and D_2O.

B. Photoelectron spectrum at 400 and 800 nm probe wavelength

In Figures 5(a) and 5(b), we show a comparison of temporally integrated spectra for pump-probe delays >5 ps. In this case, spectra were measured for aqueous NaBr solutions with 400 nm and 800 nm probe wavelength. One-color signals have been subtracted. At delay times >5 ps, the excited species is already thermalized. Sample concentrations were 30 mM NaBr (800 nm probing) and 100 mM NaBr (400 nm probing) in H_2O. The spectra are well reproduced by a single Gaussian band or the sum of two bands as indicated by the full red and green lines in Fig. 5. The spectrum obtained with 400 nm probe pulses consists of a main band peaking at a kinetic energy of (0.55 $\pm$ 0.05) eV. With 800 nm probe pulses, two bands at (0.61 $\pm$ 0.05) eV (FWHM = 0.4 eV) and (1.16 $\pm$ 0.05) eV (FWHM = 1.1 eV) appear.

The feature at 0.55 eV seems to be generated by absorption of $nh\nu$ = 3.1 eV, i.e., by a one-photon process (n = 1) in case of the 400 nm (3.1 eV) probe pulses and by a two-photon process (n = 2) in case of the 800 nm (1.55 eV)

probe pulses. The second contribution to the 800 nm probe pulse spectrum must arise from a three-photon process ($n = 3$, $nh\nu = 4.65$ eV), which cannot occur with the 400 nm probe pulses. The IR intensity dependence of the ratio of both signals (not shown here) also shows that the feature at larger kinetic energies is generated by one more IR photon than the feature at lower kinetic energies. The spectrometer shows only a mild falloff for detection efficiencies at kinetic energies <0.2 eV, hence the low energy signal is not truncated by the spectrometer. However, we have to discuss a possible influence by energy-dependent cross sections near the threshold. Let us assume for a moment that the feature at $E_{\mathrm{kin}} \sim 0.55$ eV results from a part of the broad photoelectron distribution of the conventional hydrated electron centered at the virtual energy $E_{\mathrm{kin}} \sim -0.3$ eV, where the fall-off for $E_{\mathrm{kin}} < 0.55$ eV is caused by a significantly reduced number of detected photoelectrons. In the sub-picosecond region, the time dependence of the vertical detachment energy found in I^- – water clusters[29] shows a qualitatively similar dependence as in Fig. 4. According to the Wigner law,[30] the one-photon detachment cross section near the threshold is proportional to $E_{\mathrm{kin}}^{3/2}$ for a spherically symmetric excess charge distribution. However, we are convinced that anion photodetachment as an origin of the feature at 0.55 eV is less plausible: Due to the dipole selection rules, for two-photon photodetachment, the outgoing electron is of s-type, characterized by the threshold behavior $E_{\mathrm{kin}}^{1/2}$. Thus, in the two-photon process, the slope of the number of electrons above threshold is much steeper, and the maximum of the photoelectron signal should be shifted to lower kinetic energies. In point of fact, the photoelectron signal using probe photons of 1.55 eV photon energy (cf. Fig. 5(b)) is practically the same as in the 3.10 eV probe case (cf. Fig. 5(a)) in the region $E_{\mathrm{kin}} < 0.5$ eV. Indeed, if the two spectral features arose from the same species, their intensity ratio would be independent of the salt concentration, additional iodide concentration, or delay for instance. As we will show in the next paragraph, their intensity ratio strongly depends on the salt concentration. Besides, we will show that the low kinetic energy feature is suppressed by the addition of iodide. This evidently supports our interpretation that the feature at $E_{\mathrm{kin}} \sim 0.55$ eV is not related to the conventional hydrated electron. We can now give values for the vertical ionization energies of the excited state: the feature peaking at 0.55 eV is due to a species with VIE = (2.55 ± 0.1) eV, the feature peaking at 1.16 eV is due to a species with a VIE of 3.5 eV. The latter value is very similar to the binding energy of the solvated electron. Experimentally determined values are between 3.3 eV and 3.7 eV (Refs. 9, 11, 12, and 31).

In Fig. 5(c), we show the time-dependence of the integral photoelectron signal of the 100 mM aqueous NaBr solution (probed with 400 nm pulses). The signal decays with a lifetime of (580 ± 30) fs. About 3% of the signal is due to a long-lived component.

C. Influence of salt concentration

Investigating the solute concentration dependence of the photoelectron signal will allow conclusions on the origin of the photoelectrons. If the photoreaction is independent of the solute, we do not expect that the photoelectron signal changes significantly when the solute concentration is varied in a moderate range. In Fig. 6, we show the time-integrated photoelectron spectra (5 ps ≤ Δτ ≤ 65 ps) for two different concentrations of aqueous potassium fluoride (KF) solution at identical laser conditions. While the 30 mM solution shows a very similar photoelectron spectrum as the 30 mM NaBr solution (cf. Fig. 5(b)), the 10 mM solution has a distinctly different spectrum. First, the contribution at low kinetic energies (VIE ∼ 2.5 eV) is significantly reduced compared to the part at higher kinetic energies (VIE ∼ 3.5 eV). Second, the overall signal is significantly lower. This clearly shows that the signal is solute dependent and does not arise from pure water.

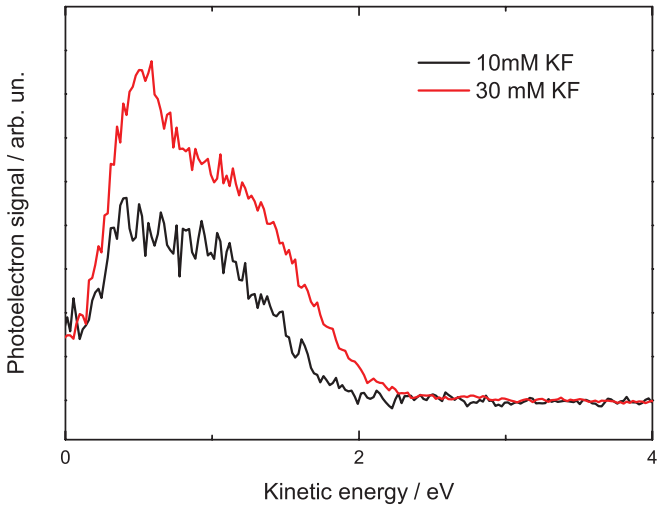

FIG. 6. Time-integrated photoelectron spectrum (5 ps ≤ Δτ ≤ 65 ps) for potassium fluoride solution of different concentrations. Pump pulse: 160 nm (7.75 eV); probe pulse: 800 nm (1.55 eV). Pump and probe intensities were identical for both spectra.

We would expect a signal proportional to the bulk concentration if the signal arose from the bulk, and we would expect deviations from this proportionality if the signal arose from the interfacial region. Due to the surface propensity of large anions, the anion surface concentration follows Langmuir isotherms and strongly influences the cation interfacial concentration.[32] We find the contribution at lower kinetic energies for the 10 mM KF solution to be a factor of ∼2 smaller than the corresponding signal of the 30 mM KF solution. The contribution at larger kinetic energies is reduced only by a factor of ∼1.5. This is an indication that both signals are generated in different regions close to the interface, where the ion density varies non-proportionally with the bulk concentration.

D. Solute dependence

In order to gain more insight into the mechanisms leading to the generation of a species with VIE ∼ 2.5 eV, we performed anion and cation dependent measurements. Results for time-integrated spectra (5 ps ≤ Δτ ≤ 65 ps) are shown in Figure 7. We also show Gaussian fits to the spectra taking two contributions into account. The photoelectron spectra for NaBr, NaCl, and KF are qualitatively similar. The peak

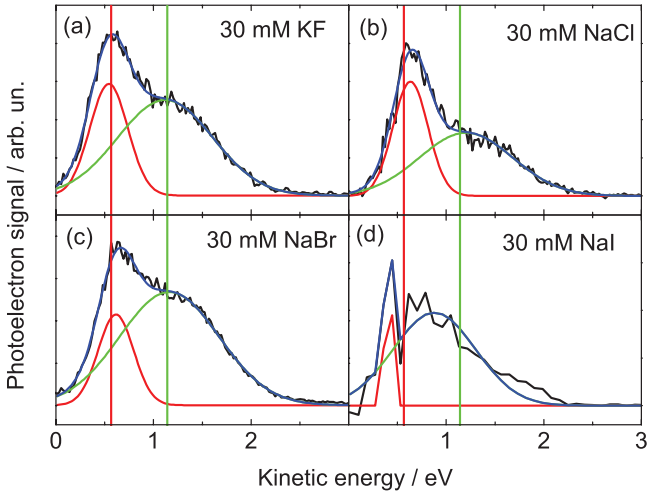

FIG. 7. Time-integrated photoelectron spectrum (5 ps $\leq \Delta\tau \leq$ 65 ps) for different salt solutions: (a) 30 mM KF, (b) 30 mM NaCl, (c) 30 mM NaBr, (d) 30 mM NaI. Pump pulse: 160 nm (7.75 eV); probe pulse: 800 nm (1.55 eV).

position of the photoelectron band at larger kinetic energies is independent of the solute. But the lower energy photoelectron band for the KF solution is shifted by about 100 meV toward smaller kinetic energies with respect to that in the spectra of NaBr and NaCl. That is, this species is stronger bound in the KF solution than in the NaCl or NaBr solution.

The fact that the VIE of the weakly bound species does not depend on the anion, but is influenced by the cation choice indicates that the observed species is spatially close (or bound to) the cation.

Even though the anion (F^-, Cl^-, Br^-) does not influence the peak positions of the photoelectron bands, i.e., the VIE, it determines the relative intensities of cation related signal to the signal peaking at 3.5 eV ionization energy. We determine $I(\text{VIE} \sim 2.5\,\text{eV})/I(\text{VIE} \sim 3.5\,\text{eV}) = 0.47 \pm 0.03$ for KF, 0.68 $\pm$ 0.07 for NaCl, and 0.29 $\pm$ 0.01 for NaBr.

The VIE of the stronger bound species (VIE $\sim$ 3.5 eV) is independent of the solute even though the concentration dependence from Fig. 6 clearly shows that this species originates from the solute.

Our observations can be explained with the assumption of an interfacial hydrated alkali cation electron complex $(M^+ \ldots e^-)_{aq}$, which is responsible for the signal with the VIE of 2.5 eV, while the signal at VIE = 3.5 eV is due to the conventional solvated electron generated by the excitation of higher CTTS states of the halides.

To explain the solute dependence of the signal ratio of the two species, we consider the influence of the solute on the surface structure. The cation and anion density in the interfacial region is a function of their surface affinity. Second harmonic generation at interfaces, as well as molecular dynamics (MD) simulations, show that for NaI, NaBr, and NaCl, the halide concentration at the interface is enhanced with the effect being largest for iodide,[32–34] while the Na^+ ions are repelled from the surface. The surface concentration of iodide solutions saturate in the mM range.[35] In NaF, no surface-enhancement of either ion is predicted by the MD simulations.[33] The specific (Hofmeister) interaction between anions and cations at the interface may disturb the formation of the interfacial $(M^+ \ldots e^-)_{aq}$ complex in case of the larger anions.

While the work of Petersen *et al.* supports our interpretations, recent photodetachment spectroscopy of aqueous salt solutions indicates that a noticeable iodide surface enhancement occurs only at a molar range.[36,37] Unfortunately, no data are available at low concentrations. Enami *et al.* used surface-sensitive electrospray mass spectrometry of μM salt solutions to show that specific ion interactions affect the ion distribution at aqueous interfaces at salt concentrations as low as 0.1 μM (Ref. 38).

The photoelectron spectrum of aqueous NaI solution (Fig. 7(d)) differs significantly from that of the other solutions. The photoelectron kinetic energies are shifted to smaller values. The existence of two distinct photoelectron bands in this case is not clear. These observations support the model introduced above: For iodide, we expect the largest surface enrichment, i.e., the strongest influence on the surface structure of the liquid jet. Thus, the formation of a hydrated $(\text{cation} \ldots e^-_{solv})$ complex is almost completely suppressed. The noisier data for iodide are due to a much higher one-color signal: photodetachment of iodide is possible with one-photon of 7.75 eV. After subtraction of the one-color signal (from the two-color signal of a quality similar to the other solutions), the resulting pump-probe spectra display a significantly higher noise level. A large energy binning was used in this case.

E. Effect of iodide addition

We used the strong effect of iodide on the spectral feature at low kinetic energies to test our model of a $(M^+ \ldots e^-)_{aq}$ complex in the interfacial region by investigating the photoelectron spectra of mixed solutions. In Figs. 8(a)–8(c), we show the photoelectron spectra of mixed solutions containing additional 30 mM of iodide. The addition of iodide changes

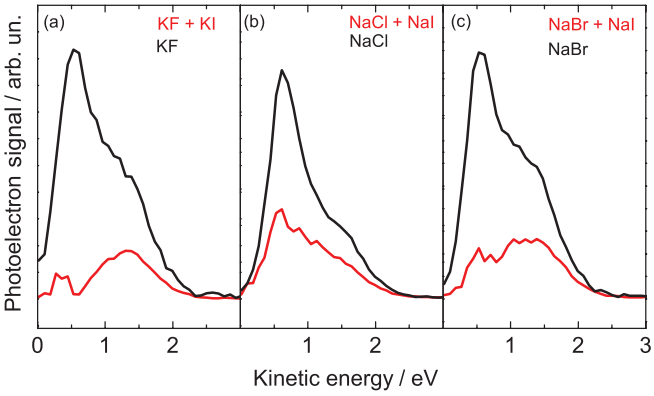

FIG. 8. Effect of iodide addition on the time-integrated photoelectron spectrum (5ps $\leq \Delta\tau \leq$ 65 ps) of different alkali halide solutions. Iodide addition suppresses the low kinetic energy part of the photoelectron spectrum. Sample concentrations were 30 mM for each simple alkali halide solution. For the mixed solutions, 30 mM of the simple alkali halide and 30 mM of the alkali iodide were used. Pump pulse: 160 nm (7.75 eV); probe pulse: 800 nm (1.55 eV).

the intensity ratio between the two contributions significantly. We find values of $I(\text{VIE} \sim 2.5\,\text{eV})/I(\text{VIE} \sim 3.5\,\text{eV}) = 0.13 \pm 0.01$ for KF+KI, 0.24 ± 0.02 for NaCl+NaI, and 0.126 ± 0.01 for NaBr + NaI.

The effect of iodide addition is strongest for KF, where the $(M^+\ldots e^-)_{aq}$ complex signal, compared to the signal at larger VIE (cf. Sec. III D), is reduced by a factor of 3.6. The effect is weakest for NaBr, where the $(M^+\ldots e^-)_{aq}$ complex signal is reduced by a factor of 2.3. This observation meets the expectations of our model: iodide will easily suppress the formation of the $(M^+\ldots e^-)_{aq}$ complex at the interface in case of KF, while the larger surface affinity of bromide will limit the effect of iodide addition. If the low energy species would stem from a bulk species, we would not expect significant effects upon iodide addition.

IV. *AB INITIO* CALCULATIONS ON SODIUM-WATER CLUSTERS

The experimentally observed signal at low kinetic energies shows the binding energy to be dependent on the cation. In the following, we describe quantum chemical computations on the geometry and energetics of $Na^+(H_2O)_{20}$ and $Na(H_2O)_{20}$ clusters to identify possible "nano"-species carrying the essential properties for our model to explain the observed signals with VIE ~2.5 eV. Here, the cationic cluster $Na^+(H_2O)_{20}$ is the initial species, used for the description of the photoexcitation process. After excitation, the created positively charged valence hole rapidly diffuses away. Assuming that the orientation of the water molecules remains unchanged during this process, after some time, our "central unit" can be treated as a neutral $Na(H_2O)_{20}$ cluster, if the valence hole as well as the positive charge is located outside. To evaluate the structural evolution of ground state $Na(H_2O)_{20}$ clusters, we have carried out classical molecular dynamics simulations.

A. Computational details

The *ab initio* calculations of the clusters are performed using the TURBOMOLE program package.[39] Geometry optimizations and ground state energy computations are done with the help of the resolution-of-identity second order Møller-Plesset (RI-MP2) method;[40] for the determination of excitation energies, the resolution-of-identity second-order approximate coupled-cluster (RI-CC2) method[41] is used. For oxygen and hydrogen, the augmented correlation-consistent polarized valence double-zeta (aug-cc-pVDZ) (Refs. 42 and 43) and for the alkali atom, the valence triple-zeta plus polarization (TZVP) (Refs. 44 and 45) basis sets are used.

Classical *ab initio* molecular dynamics calculations are performed at the Multipole-Accelerated-Resolution-of-Identity-J (MARI-J) density functional theory (DFT) level,[46] using the Becke three parameter Lee-Yang-Parr (B3LYP) functional and the TZVP (Ref. 47) basis set for all atoms. The dispersion interaction is considered in a semiempirical way.[48] The cluster system is coupled via a Nosé-Hoover thermostat[49,50] to a bath characterized by the temperature $T = 300$ K. The time step for the integration of the Newtonian equations of motion is 1 fs.

TABLE I. Calculated energetics of four low-lying isomers of $Na^+(H_2O)_{20}$. The ground-state energy W_g of the lowest isomer (I) is set to zero. W_{ex} is the lowest optical excitation energy (relative to W_g), $\mu_{g\to ex}$ the corresponding transition dipole moment, and W_{EA} denotes the electron affinity.

	W_g (eV)	W_{ex} (eV)	$\mu_{g\to ex}$ (Debye)	W_{EA} (eV)
I	0.00	7.97	0.63	2.06
II	0.18	7.74	1.10	2.21
III	0.19	7.73	1.12	2.23
IV	0.22	7.68	1.19	2.30

B. Results

The water cluster $(H_2O)_{21}$ consists of 20 water molecules located at the edges of a distorted dodecahedron and one molecule in the center (one-centered cage). This is a magic cluster due to the relatively high binding energy per molecule.[51,52] Furthermore, its structure is nearly spherical and therefore it is a good candidate for testing a continuum model using a dielectric sphere.

Next, we have replaced one water molecule near the cluster surface by a sodium cation and carried out a RI-MP2 geometry optimization. Several local minima have been found with geometries differing essentially by the direction of the OH bonds relative to the cation and the surface. In Table I, the calculated energetics (ground state energy W_g, lowest vertical excitation energy W_{ex}, transition dipole moment $\mu_{g\to ex}$, and vertical electron affinity W_{EA}) of four low-lying isomers (I–IV) are shown. For comparison, we have also calculated the vertical excitation energy of a single water molecule. Within our level of theory (RI-CC2, aug-cc-pVDZ basis set), we have found a value 7.04 eV for the $\tilde{X} \to \tilde{A}$ transition. The experimental spectrum peaks at 7.45 eV (Ref. 2). We may therefore expect that the W_{ex}-values given in Table I underestimate the real optical excitation edges by a few tenth of eV. On the other hand, the first excited state of the $Na^+(H_2O)_{20}$ cluster is of charge transfer character $(Na^+\ldots e^-)(H_2O^+)(H_2O)_{19}$ – one electron is transferred from one water molecule to the cluster surface above the sodium cation, and populating the lowest unoccupied orbital (LUMO) that is very similar to the singly occupied molecular orbital (SOMO) of neutral $(Na^+\ldots e^-)(H_2O)_{20}$. This is also manifested in the observation that the electron affinity W_{EA} increases with decreasing excitation energy W_{ex}. The electron density of the unpaired electron of the $(Na^+\ldots e^-)(H_2O)_{20}$ cluster (geometry of isomer II) is shown in Fig. 9. The excitation creates a valence hole in the water network at a distance of 9–13 a.u. to the center of the charge distribution of the excited electron. In spite of this large charge separation, the transition dipole moments for the HOMO → LUMO transition are not small (cf. Table I).

V. EXTRAPOLATION OF THE ENERGETICS FROM THE CLUSTER TO THE SURFACE OF THE LIQUID

In order to extrapolate the calculated properties of a finite cluster to properties of the condensed phase, we take advantage of the dielectric continuum model[53–56] approximating the cluster by a dielectric sphere of radius R. Within the limit

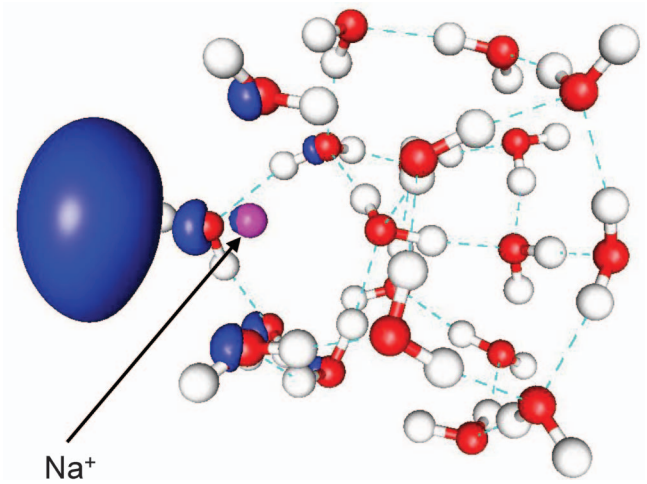

FIG. 9. Equilibrium geometry of the cationic cluster isomer II including the spin density (blue color) of the neutral cluster after electron attachment.

$R \rightarrow \infty$, we hope to obtain a qualitative description of the nature of the water/vacuum interface. Here, we rely on an assumption that the local environment around the excited electron and the alkali cation remains roughly unchanged if the size of the dielectric sphere R increases. The necessary basic mathematical expressions to evaluate the vertical transition energy are listed in Chapter I of the supplementary material.[57]

A. Parametrization of the dielectric continuum model

First, we want to approximate the electrostatic properties of the $Na^+(H_2O)_{20}$ cluster by a positive point charge inside a dielectric sphere. After geometry optimization for all four isomers, we find a distance $r_c \sim 5.3$ a.u. between the sodium cation and the cluster center. Fitting the electrostatic potential outside the cluster (obtained from our *ab initio* calculations above), with the expression for a point charge within a dielectric sphere (details are given in the supplementary material (Ref. 57)), we find $\epsilon_s \sim 8$ for the relative static permittivity. This value is considerably lower than that of bulk water. However, the large value $\epsilon_s \sim 80$ in the liquid is mainly associated with the presence of the underlying hydrogen-bond network.[58] Our cluster consists of only one central water molecule, the other water molecules are located at the surface, where the coordination number is reduced. In this, our calculations agree with the significantly lower permittivities $\epsilon_s < 10$ that were experimentally observed near water/mica[59] and also water/air interfaces.[60,61]

Next, we use the fixed value $\epsilon_s = 8$ and search for the radius R, where the fit of the *ab initio* electrostatic potential performs a transition from the region outside to inside the dielectric sphere. We have obtained a value $R \sim 10.5$ a.u. arising from the Wigner-Seitz radius of 3.8 a.u. for a water molecule (cf., e.g., Ref. 62). This value is also a good value for the radius R of the dielectric sphere model. It must be mentioned that this radius is so large that all nuclei of the cluster are located *inside* the dielectric sphere. Moreover, they are at least 1 a.u. away from the dielectric surface.

To allow the determination of the electronic part of the water cluster permittivity ϵ_{el} and the position of the negative charge, the electrostatic potential outside of a neutral $(Na^+ \ldots e^-)(H_2O)_{20}$ cluster with the same geometry is studied by quantum-chemical computations. We have obtained $\epsilon_{el} \sim 1.7$ correlating with the well-known refractive index of water ice ($n = 1.31$). For the determination of the electrostatic potential outside the cluster, the attached electron can be approximately treated as a negative point charge localized at the cluster surface above the sodium ion core.

B. Behavior of the transition energy to the first excited electronic state

After calculating the first excited electronic state of the $Na^+(H_2O)_{20}$ clusters, we estimated the change of the excitation energy if the cluster radius R becomes infinitely large. From our *ab initio* calculations, we found that the optical excitation leads to a charge separation: A surface electron is formed, spatially separated from the cationic core. Additionally, the sodium cation is present in the ground as well as in the excited electronic state. In Chapter II of the supplementary material,[57] the extrapolation $R \rightarrow \infty$ is carried out to estimate the behavior of the VUV absorption edge. This is done for the three different values of static surface permittivity ϵ_s. According to Chapter II of the supplementary material,[57] the difference between the excitation energy at the surface of the liquid and that of the cluster ($\Delta W_{\text{surf}-\text{clust}}$) is given by

$$\Delta W_{\text{surf - clust}} = \begin{cases} +0.1 \ldots + 0.2 \text{ eV} & \text{if} \quad \epsilon_s = 80 \\ -0.4 \ldots - 0.3 \text{ eV} & \text{if} \quad \epsilon_s = 8 \\ -0.8 \ldots - 0.6 \text{ eV} & \text{if} \quad \epsilon_s = 4\,. \end{cases} \tag{2}$$

The optical excitation energy at the surface of liquid water in the vicinity of a sodium cation decreases significantly with decreasing static surface permittivity. As mentioned above, the cluster excitation energies W_{ex}, given in Table I, underestimate the true excitation energies. If we now consider the extrapolation to the liquid state with $\epsilon_s = 80$ according to Eq. (2), we find that the excitation edge is well above the pump photon energy of 7.75 eV. For lower permittivities in the surface region, optical excitation should be possible. The theoretical results therefore suggest that a suitable choice of excitation energy may lead to the selective excitation of surface states.

C. Estimation of the vertical ionization energies

The behavior of the VIE of the optically created hydrated $(Na^+ \ldots e^-)$ pair as a function of pump-probe delay τ is discussed in more detail in Chapter III of the supplementary material.[57] Here, the increase of the permittivity $\epsilon(\tau)$ with time $[\epsilon_{el} < \epsilon(\tau) \leq \epsilon_s]$ plays an essential role because this magnitude describes the increasing polarization of water when time proceeds due to the creation of the additional charge of an electron and the positively charged valence hole. If we denote the electron radius by a and the distance of the electron charge center to the charge of the valence hole by d_{we}, the τ-dependence of VIE can be expressed in atomic units as follows (for details see Chapter III.C of the supplementary

material[57]):

$$\mathrm{VIE}(\tau) = \mathrm{VIE}^*(0) + \left[\frac{1}{\epsilon_{el}+1} - \frac{1}{\epsilon(\tau)+1}\right]\frac{1}{a} + \frac{2}{[\epsilon(\tau)+1]\,d_{we}}. \quad (3)$$

Here, $\mathrm{VIE}^*(0)$ is the "virtual" vertical ionization energy at $\tau = 0$, where the positive charge of the valence hole is not taken into account.

Under the assumption that the distance between water cation and electron, d_{we}, is τ-independent and is sufficiently large ($d_{we} > 2a$), the vertical ionization energy monotonically increases with increasing pump-probe delay τ. This behavior is experimentally observed for $\tau > 100$ fs (cf. Fig. 4(a)). The decrease of VIE with raising τ—measured for $\tau < 100$ fs—arises from the crucial role of the last term in Eq. (3): due to charge diffusion, the mean value of d_{we} rapidly increases. As discussed in the supplementary material, the best agreement with the experimental course of $\mathrm{VIE}(\tau)$ is achieved if the magnitude $\epsilon(\tau)$ is confined by the upper limit $\epsilon_s \sim 8$. It must be noted that for our qualitative discussion, we have assumed a fixed d_{we}-value—a more rigorous treatment of its (realistic) time dependence leads to a spatial dependence of $\epsilon(\tau)$ and is beyond the scope of the present paper.

VI. DISCUSSION OF THE PHOTOINDUCED DYNAMICS

We now briefly discuss the migration of the positive charge localized on a water molecule immediately after the pump pulse action. An ionized water molecule is not stable in a water environment, an ultrafast proton transfer reaction occurs,[1,63]

$$H_2O + H_2O^+ \rightarrow H_3O^+ + OH. \quad (4)$$

According to *ab initio* calculations for the ground state of the water dimer cation,[64] the valence hole is initially strongly localized on the hydrogen-bond donating monomer; a proton can easily transfer to the neutral monomer. As quantum mechanical wavepacket calculations have shown, this formation of the hydronium cation is faster than 50 fs (Ref. 64). In our RI-CC2 calculations of the $Na^+(H_2O)_{20}$ cluster, we have found that such a proton transfer reduces the energy of the relevant first excited electronic state by more than 1 eV. We may expect that this large amount of excess energy induces a fast proton migration, leading to a rapid increase of the mean d_{we}-value. As reflected in Eq. (3), this causes the initial decrease of ionization energy visible in Figs. 3 and 4(a). Because the proton hopping is of diffusive character, there is some probability for a proton transfer induced electron quenching reaction:

$$H_3O^+ + e^- \rightarrow H_2O + H^+ \ldots e^- \rightarrow H_2O + H. \quad (5)$$

This process has been theoretically studied by molecular dynamics simulations of a cluster consisting of 32 water molecules, one proton, and one electron.[65] Thirty percent of the simulated trajectories lead to a quenching reaction within 3.5 ps. Due to the different migration velocity of H^+ and D^+, the quenching of the photoelectron signal on the basis of reaction (5) should be faster in H_2O than in D_2O. As a distinct isotope effect of the short-lived ion signal (cf. Fig. 4(b)) has been found, this reaction may contribute to the signal quenching on the sub-picosecond time scale.

In the primary reaction (4) also, the radical OH is formed. If it is located near the surface electron, the electron attachment process,

$$OH + e^- \rightarrow OH^-, \quad (6)$$

is relevant for the decrease of the photoelectron signal. Recently, Car-Parrinello molecular dynamics simulations of the hydroxyl radical in liquid water (utilizing different system sizes of 31 and 63 water molecules) have been carried out.[66] There, it has been emphasized that the very rapid H-transfer reaction significantly contributes to the high mobility of OH radicals in aqueous solution. This implies a pronounced isotope effect of the OH/OD diffusion constant. Thus, reaction (6) may also be responsible for the observed isotope effect of the signal lifetime seen in Fig. 4(b).

We want to note that a halogen anion can act as an OH or H^+ scavenger. Thus, the reactions (5) and (6) may be suppressed. As in our experiments, the surface concentration of $(Br^-)_{aq}$ is higher compared with $(Cl^-)_{aq}$, our observed subpicosecond lifetime of the $(Na^+\ldots e^-)_{aq}$ complex is longer for NaBr than for NaCl solutions.

In our own molecular dynamics simulations of the neutral $Na(H_2O)_{20}$ cluster up to 5 ps, the distance between the sodium cation and the surface electron is approximately conserved; we cannot provide any evidence of the development of the most stable configuration - two separate solvation centers [$(Na^+)_{aq}$ and $(e^-)_{aq}$]. Calculations of the minimum structure of the $Na(H_2O)_{20}$ complex[67] yielded a solvated electron near the surface and a sodium cation near the surface on the other side of the cluster. Probably, in our case, the barrier to this configuration is too high, so that a transition needs much more time. Furthermore, the $Na(H_2O)_{20}$ cluster is too small for a proper description of an internally hydrated electron. Therefore, it may be possible that the formation of two solvation centers from the surface-solvated $(Na^+\ldots e^-)$ contact pair proceeds faster in the liquid phase.

The proton migration (diffusion), triggered by the creation of a valence hole in the water network, is strongly dependent on temperature.[68] Due to the initial high kinetic energy of the proton (see above), the first few hops should be very fast, but after thermalization (to $T = 300$ K), the diffusion constant is reduced to $D \sim 10^{-4}\mathrm{cm}^2\mathrm{s}^{-1}$ (Ref. 68). Consequently, for longer time delays ($\tau > 500$ fs), it is difficult to determine whether there is a significant contribution of the last term in Eq. (3). In this regard, a comparison of the H_2O/D_2O ionization energies is interesting. Our experiments show that the ionization energy in heavy water is 0.1−0.15 eV higher than in light water (see Fig. 4(a)). Note that this is not an ordinary isotope shift typical for vibronic transitions, because water is not ionized. Here, the isotope effect is mainly caused by the H/D mass difference: As the deuteron migration velocity is smaller than that of a proton, the initial ($\tau < 100$ fs) increase of the electron kinetic energy is less pronounced in D_2O than in H_2O. This may also be an indication for a generally larger influence of the deuteron charge (smaller average d_{we}-value) on the measured ionization energy for larger

delay times τ. In addition, there may be a (somewhat smaller) contribution of another isotope effect, present already at $\tau = 0$: The absorption band of liquid D_2O is blue-shifted relative to that of H_2O (Ref. 3). Therefore, we expect that a given pump photon energy excites different isomeric structures in heavy water. According to Table I, isomers with low excitation energy show larger electron affinities (and higher ionization energies, if the valence hole is not taken into account). This behavior persists as long as the interconversion of the different isomers is not finished during the pump-probe delay. Our molecular dynamics simulations predict a 500 fs interconversion time between the isomers (reorientation of the OH-bonds at the surface). To clarify the influence of the absorption band position, it is therefore highly desirable to vary the pump photon energy in a future work.

VII. CONCLUSIONS

After irradiating a liquid microjet of different aqueous alkali halide solutions with an optical pulse of 7.75 eV photon energy (160 nm) and sub-20 fs duration, we have probed ultrafast solvated electron dynamics on the sub-picosecond time scale. The photoelectron signal increases with the solute concentration (not proportionally) and we observe two contributions when probing at 800 nm. The VIE of the weaker bound species (~2.5 eV) shows a slight dependence on the cation choice, while the VIE of the stronger bound species (~3.5 eV) does not vary with the solute. However, the solute determines the signal strength. The anion influences the relative intensities of the two contributions. The formation of both species is suppressed by the addition of iodide, the weaker bound species being more affected.

From these experimental observations, we conclude that—regarding the creation of the weakly bound species—the primary photoexcitation step occurs in the solvent shell of a cation. Near the surface, the lowest excited electronic state is a charge-transfer state, where the excited electron resides above the alkali cation, as found by our *ab initio* calculations for the $Na^+(H_2O)_{20}$ cluster. At the liquid/vacuum interface, after the pump pulse action, the initial positive charge located at one or two water molecules rapidly diffuses away due to proton migration. This process is reflected in the measured initial ($\tau < 100$ fs) VIE decrease.

For larger pump-probe delays, we observe a VIE increase due to the domination of solvent shell equilibration. We qualitatively describe the subsequent stabilization of the $(Na^+\ldots e^-)_{aq}$ complex on the basis of a dielectric continuum model. The surface electron is not only stabilized due to its polarization of the water surface layer, but also as a result of the incomplete dielectric screening of the Coulombic $Na^+\ldots e^-$ interaction. Whereas in the bulk, the static relative permittivity ϵ_s of liquid water is about 80, the comparison of experimental and calculated data indicate that this value is about one order of magnitude smaller near the surface, leading to a substantially weaker screening of solvated charged species. If we set $\epsilon_s = 8$ and assume a distance $d_c = 5.2$ a.u. between the alkali cation and the charge center of the electron [the distance of the sodium nucleus to the cluster surface found for $Na^+(H_2O)_{20}$], we obtain an electrostatic interaction energy at the surface $W_{int} = 2/[(\epsilon_s + 1)\, d_c] = 0.0427$ a.u. $\equiv 1.16$ eV. In a study of very cold $(H_2O)_n^-$ clusters, two types of surface-bound excess electrons were found:[69] One, characterized by an extrapolated ($n \to \infty$) vertical binding energy of ~0.3 eV, and the other by ~1.6 eV. On the basis of recent molecular dynamics simulations,[70] the former can be associated with a "dipole-bound" electron of large radius of gyration, the latter with a more localized "proper surface isomer" (cf. Fig. 3 in Ref. 70). Adding the interaction energy W_{int} to the extrapolated electron binding energy 1.6 eV, we obtain a value that is near to our observed ionization energy of (2.55 ± 0.1) eV. We therefore postulate that the cation attraction stabilizes the localized surface isomer, allowing the observation of the solvated $Na^+\ldots e^-$ complex also on the liquid surface at ambient temperatures.

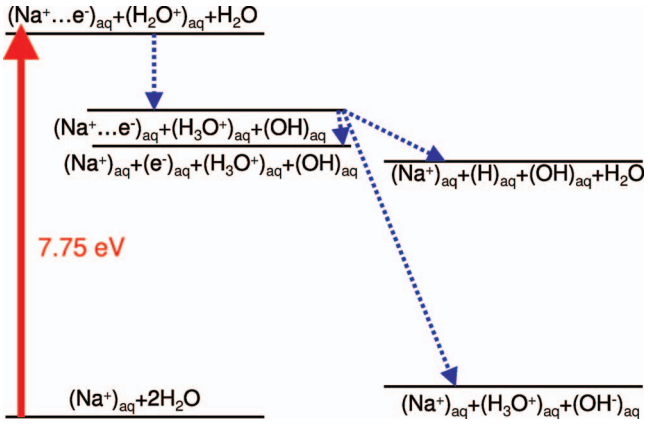

FIG. 10. Proposed photoinduced processes after the optical excitation of a surface-hydrated sodium-cation/electron complex. The energetic positions of the four lowest levels are shown according to Coe[71] and Han *et al.*[72] The highest two levels are shown tentatively—on the basis of our own estimations.

The surface complex $(Na^+\ldots e^-)_{aq}$ may decay along the channels proposed in Fig. 10. In the sub-picosecond time scale, the observed H/D isotope effect of the $(Na^+\ldots e^-)_{aq}$ lifetime is in agreement with the electron capture reactions (5) and (6). The formation of the conventional solvated electron $(e^-)_{aq}$ as a decay product of $(Na^+\ldots e^-)_{aq}$ is only a minor channel. Mainly, the $(e^-)_{aq}$ species is initially produced due to photodetachment of solvated halogen anions.

Recently, a theoretical investigation on the microhydration of a delocalized solvent-separated $H_3O^+\ldots e^-$ pair was reported;[73] the structure for the $H_3O(H_2O)_3$ cluster is similar to a sub-structure of our $Na(H_2O)_{20}$ complex, if hydronium is replaced by sodium. Of further interest is the report[74] that a sodium cation placed on a surface of amorphous D_2O ice layers leads to a faster energetic stabilization of the solvated electron: a transient electron/alkali-ion/water complex at the ice/vacuum interface is formed and may be related to the $(Na^+\ldots e^-)_{aq}$ complex discussed here.

Summarizing, we have qualitatively described the processes occurring after the VUV excitation of a water/vacuum interface in the presence of alkali cations. To get a deeper insight, it would be helpful to tune the pump photon energy around 7.75 eV with the aim to detect the formation edge of the surface-solvated $Na^+\ldots e^-$ complex and to obtain the

onset of the region where the excitation of bulk water dominates. Work on a corresponding tunable VUV source is currently underway.

ACKNOWLEDGMENTS

The authors thank F. Noack for his support by providing the laser system in the femtosecond application laboratory of the Max-Born-Institut, Berlin. This work was supported by the Deutsche Forschungsgemeinschaft, Project LU 1638/1-1.

[1] B. C. Garrett, D. A. Dixon, D. M. Camaioni, D. M. Chipman, M. A. Johnson, C. D. Jonah, G. A. Kimmel, J. H. Miller, T. M. Rescigno, P. J. Rossky, S. S. Xantheas, S. D. Colson, A. H. Laufer, D. Ray, P. F. Barbara, D. M. Bartels, K. H. Becker, K. H. Bowen, Jr., S. E. Bradforth, I. Carmichael, J. V. Coe, L. R. Corrales, J. P. Cowin, M. Dupuis, K. B. Eisenthal, J. A. Franz, M. J. Gutowski, K. D. Jordan, B. D. Kay, J. A. LaVerne, S. V. Lymar, T. E. Madey, C. W. McCurdy, D. Meisel, S. Mukamel, A. R. Nilsson, T. M. Orlando, N. G. Petrik, S. M. Pimblott, J. R. Rustad, G. K. Schenter, S. J. Singer, A. Tokmakoff, L.-S. Wang, C. Wittig, and T. S. Zwier, Chem. Rev. **105**, 355 (2005).
[2] R. Mota, R. Parafita, A. Giuliani, M.-J. Hubin-Franskin, J. M. C. Lourenço, G. Garcia, S. V. Hoffmann, N. J. Mason, P. A. Ribeiro, M. Raposo, and P. Limão Vieira, Chem. Phys. Lett. **416**, 152 (2005).
[3] A. Ikehata, N. Higashi, and Y. Ozaki, J. Chem. Phys. **129**, 234510 (2008).
[4] P. C. do Coto and D. M. Chipman, J. Chem. Phys. **132**, 244307 (2010).
[5] C. G. Elles, I. A. Shkrob, R. A. Crowell, and S. E. Bradforth, J. Chem. Phys. **126**, 164503 (2007).
[6] H. T. Liu, J. P. Müller, M. Beutler, M. Ghotbi, F. Noack, W. Radloff, N. Zhavoronkov, C. P. Schulz, and I. V. Hertel, J. Chem. Phys. **134**, 094305 (2011).
[7] F. Buchner, T. Schultz, and A. Lübcke, Phys. Chem. Chem. Phys. **14**, 5837 (2012).
[8] F. Buchner, A. Lübcke, N. Heine, and T. Schultz, Rev. Sci. Instrum. **81**, 113107 (2010).
[9] A. Lübcke, F. Buchner, N. Heine, I. V. Hertel, and T. Schultz, Phys. Chem. Chem. Phys. **12**, 14629 (2010).
[10] Y. Tang, Y.-I. Suzuki, H. Shen, K. Sekiguchi, N. Kurahashi, K. Nishizawa, P. Zuo, and T. Suzuki, Chem. Phys. Lett. **494**, 111 (2010).
[11] A. T. Shreve, T. Y. Yen, and D. M. Neumark, Chem. Phys. Lett. **493**, 216 (2010).
[12] K. R. Siefermann, Y. Liu, E. Lugovoy, O. Link, M. Faubel, U. Buck, B. Winter, and B. Abel, Nat. Chem. **2**, 274 (2010).
[13] M. J. Blandamer and M. F. Fox, Chem. Rev. **70**, 59 (1970).
[14] M. F. Fox and E. Hayon, J. Chem. Soc., Faraday Trans. 1 **73**, 1003 (1977).
[15] M. F. Fox, B. E. Barker, and E. Hayon, J. Chem. Soc., Faraday Trans. 1 **74**, 1776 (1978).
[16] H. Iglev, R. Laenen, and A. Laubereau, Chem. Phys. Lett. **389**, 427 (2004).
[17] B. Winter, R. Weber, I. V. Hertel, M. Faubel, P. Jungwirth, E. C. Brown, and S. E. Bradforth, J. Am. Chem. Soc. **127**, 7203 (2005).
[18] G. A. Laguna and W. H. Beattie, Chem. Phys. Lett. **88**, 439 (1982).
[19] H. Uehara and K. Horiai, J. Op. Soc. Am. B **4**, 1217 (1987).
[20] J. L. Tech, J. Res. Natl. Bur. Stand. **67A**, 505 (1963).
[21] W. C. Martin and C. H. Corliss, J. Res. Natl. Bur. Stand. **64A**, 443 (1960).
[22] B. Winter, R. Weber, W. Widdra, M. Dittmar, M. Faubel, and I. V. Hertel, J. Phys. Chem. A **108**, 2625 (2004).
[23] M. S. Banna, B. H. McQuaide, R. Malutzki, and V. Schmidt, J. Chem. Phys. **84**, 4739 (1986).
[24] M. Beutler, M. Ghotbi, F. Noack, and I. V. Hertel, Opt. Lett. **35**, 1491 (2010).
[25] M. Beutler, M. Ghotbi, and F. Noack, Opt. Lett. **36**, 3726 (2011).
[26] C. P. Hauri, W. Kornelis, F. W. Helbing, A. Heinrich, A. Couairon, A. Mysyrowicz, J. Biegert, and U. Keller, Appl. Phys. B **79**, 673 (2004).
[27] M. Ghotbi, M. Beutler, and F. Noack, Opt. Lett. **35**, 3492 (2010).
[28] M. Faubel and B. Steiner, Ber. Bunsenges. Phys. Chem. **96**, 1167 (1992).
[29] A. Kammrath, J. R. R. Verlet, A. E. Bragg, G. B. Griffin, and D. M. Neumark, J. Phys. Chem. A **109**, 11475 (2005).
[30] E. P. Wigner, Phys. Rev. **73**, 1002 (1948).
[31] Y. Tang, H. Shen, K. Sekiguchi, N. Kurahashi, T. Mizuno, Y.-I. Suzuki, and T. Suzuki, Phys. Chem. Chem. Phys. **12**, 3653 (2010).
[32] P. B. Petersen and R. J. Saykally, Annu. Rev. Phys. Chem. **57**, 333 (2006).
[33] P. Jungwirth and D. Tobias, J. Phys. Chem. B **105**, 10468 (2001).
[34] P. B. Petersen and R. J. Saykally, J. Am. Chem. Soc. **127**, 15446 (2005).
[35] P. B. Petersen, J. C. Johnson, K. P. Knutsen, and R. J. Saykally, Chem. Phys. Lett. **397**, 46 (2004).
[36] M. Shoji, K. Kaniwa, Y. Hiranuma, O. Maselli, and F. Mafune, J. Phys. Chem. A **115**, 2148 (2011).
[37] Y. Hiranuma, K. Kaniwa, M. Shoji, and F. Mafune, J. Phys. Chem. A **115**, 8493 (2011).
[38] S. Enami, H. Mishra, M. R. Hoffmann, and A. J. Colussi, J. Chem. Phys. **136**, 154707 (2012).
[39] R. Ahlrichs, M. Bär, M. Häser, H. Horn, and C. Kölmel, Chem. Phys. Lett. **162**, 165 (1989).
[40] F. Weigend and M. Häser, Theor. Chem. Acc. **97**, 331 (1997).
[41] C. Hättig and F. Weigend, J. Chem. Phys. **113**, 5154 (2000).
[42] D. E. Woon and T. H. Dunning, Jr., J. Chem. Phys. **100**, 2975 (1994).
[43] F. Weigend, A. Köhn, and C. Hättig, J. Chem. Phys. **116**, 3175 (2002).
[44] A. Schäfer, C. Huber, and R. Ahlrichs, J. Chem. Phys. **100**, 5829 (1994).
[45] F. Weigend, M. Häser, H. Patzelt, and R. Ahlrichs, Chem. Phys. Lett. **294**, 143 (1998).
[46] M. Sierka, A. Hogekamp, and R. Ahlrichs, J. Chem. Phys. **118**, 9136 (2003).
[47] K. Eichkorn, O. Treutler, H. Öhm, M. Häser, and R. Ahlrichs, Chem. Phys. Lett. **242**, 652 (1995).
[48] S. Grimme, J. Comput. Chem. **27**, 1787 (2006).
[49] S. Nosé, J. Chem. Phys. **81**, 511 (1984).
[50] W. G. Hoover, Phys. Rev. A **31**, 1695 (1985).
[51] A. Lenz and L. Ojamäe, Phys. Chem. Chem. Phys. **7**, 1905 (2005).
[52] Z. Yang, S. Hua, W. Hua, and S. Li, J. Phys. Chem. A **114**, 9253 (2010).
[53] R. A. Marcus, J. Chem. Phys. **24**, 979 (1956).
[54] J. Jortner, Mol. Phys. **5**, 257 (1962).
[55] R. N. Barnett, U. Landman, G. Makov, and A. Nitzan, J. Chem. Phys. **93**, 6226 (1990).
[56] G. Makov and A. Nitzan, J. Phys. Chem. **98**, 3459 (1994).
[57] See supplementary material at http://dx.doi.org/10.1063/1.4732582 for details on the extrapolation of the energetics from the cluster to the surface of the liquid.
[58] M. Sharma, R. Resta, and R. Car, Phys. Rev. Lett. **98**, 247401 (2007).
[59] O. Teschke, G. Ceotto, and E. F. de Souza, Phys. Rev. E **64**, 011605 (2001).
[60] O. Teschke and E. F. de Souza, Chem. Phys. Lett. **403**, 95 (2005).
[61] O. Teschke and E. F. de Souza, Phys. Chem. Chem. Phys. **7**, 3856 (2005).
[62] I. V. Hertel, C. Hüglin, C. Nitsch, and C. P. Schulz, Phys. Rev. Lett. **67**, 1767 (1991).
[63] O. Marsalek, C. G. Elles, P. A. Pieniazek, E. Pluhařova, J. VandeVondele, S. E. Bradforth, and P. Jungwirth, J. Chem. Phys. **135**, 224510 (2011).
[64] E. Kamarchik, O. Kostko, J. M. Bowman, M. Ahmed, and A. I. Krylov, J. Chem. Phys. **132**, 19431 (2010).
[65] O. Marsalek, T. Frigato, J. VandeVondele, S. E. Bradforth, B. Schmidt, C. Schütte, and P. Jungwirth, J. Phys. Chem. B **114**, 915 (2010).
[66] E. Codorniu-Hernández and P. G. Kusalik, J. Chem. Theory Comput. **7**, 3725 (2011).
[67] B. Gao and Z.-F. Liu, J. Chem. Phys. **126**, 084501 (2007).
[68] M. Boero, T. Ikeshoji, and K. Terakura, Chem. Phys. Chem. **6**, 1775 (2005).
[69] J. R. R. Verlet, A. E. Bragg, A. Kammrath, O. Cheshnovsky, and D. M. Neumark, Science **307**, 93 (2005).
[70] L. D. Jacobson and J. M. Herbert, J. Am. Chem. Soc. **133**, 19889 (2011).
[71] J. V. Coe, Int. Rev. Phys. Chem. **20**, 33 (2001).
[72] P. Han and D. M. Bartels, J. Phys. Chem. **96**, 4899 (1992).
[73] F. Uhlig, O. Marsalek, and P. Jungwirth, Phys. Chem. Chem. Phys. **13**, 14003 (2011).
[74] M. Meyer, M. Bertin, U. Bovensiepen, D. Wegkamp, M. Krenz, and M. Wolf, J. Phys. Chem. C **115**, 204 (2011).